Proper Determination of Ouzo Limits while Nanoprecipitating Oils

Yiping Chen, Adèle Mosa, Sacha Bouvier, Julien Bernard, François Ganachaud

Proper Determination of Ouzo Limits while Nanoprecipitating Oils

Yiping Chen, Adèle Mosa, Sacha Bouvier, Julien Bernard*, François Ganachaud*

Univ Lyon, CNRS, UMR 5223, Ingénierie des Matériaux Polymères, Université Claude Bernard Lyon 1, INSA Lyon, Université Jean Monnet, F-69621 Villeurbanne Cedex, France

Ouzo effect – emulsion – solvent shifting – supersaturation – nucleation and aggregation

ABSTRACT: The Ouzo effect is a generic technology to produce at will colloidal dispersions from a variety of solutes. Whereas phase diagrams have been quite easily derived when nanoprecipitating polymers, the case of oils is less straightforward. Indeed, the short-term stability of generated nanodroplets in water/solvent mixtures complexifies the establishment of the diagram boundaries. This article proposes two complementary methods to determine with fair accuracy Ouzo limits in ternary systems oil/solvent/non-solvent, with and without surfactant. A discussion follows on the localization and shape of the Ouzo limit .

1. Introduction

The generation of nanoparticles of many shapes and sizes is sought everywhere nowadays for applications in medicine, building, healthcare or food industries.[1] Among the different physical chemistry techniques currently available for nanoparticle preparation, the nanoprecipitation (also called 'Ouzo effect'[2]) certainly stands high for its versatility and simplicity. Indeed, any hydrophobic solute can be colloidally dispersed in water this way, sometimes even without the need of a surfactant. Hundreds of examples of polymer nanoparticles and nanocapsules, vesicles or solid aqueous nanodispersions have been prepared by this technology for more than a century (see some most recent reviews here[3,4]).

Quite surprisingly, it is as late as in 2005 that Vitale and Katz[5] have shown that the process could be experimentally described by simple pseudo-ternary phase diagrams of solute versus solvent contents (See Figure 1, the water content is deduced from the other two mass ratios). By using a log scale for the solute content, an 'Ouzo domain' was identified where nanodispersions are obtained in the full volume. Manipulating these phase diagrams nowadays allows one to generate as complex dispersions as Janus, onions or multilamellar polymer particles, for instance.[6] It also gave rise to the generation of oil-loaded polymer nanocapsules of various sizes and loads.[7,8,9]

So far a limitation of the technique is that the Ouzo domain is typically associated with very low concentrations of solute. It would thus be of interest to develop robust methods allowing for rapid identification of the boundaries in order to effectively determine the parameters that allow to shift the ouzo limit towards higher concentration in solute. Here, we present works that have been done on simple oil/solvent/water mixtures, together with a non-ionic surfactant when necessary.[10] We first explain why phase diagrams derived so far for oils are most often too rough to be exploited. Then we will present two methods to accurately generate the Ouzo limit, namely fluorescence microscopy (FM) and dynamic light scattering (DLS). We finally tentatively discuss the physical chemistry behind the derived phase diagrams.

2. A brief update on Ouzo limit determination

Various reviews have described the Ouzo effect, focusing on different aspects of the technology: anterior works,[2] application in drug delivery[3,4] or chemical engineering of microfluidic devices[11] or high-speed mixers[12]. To our knowledge, none of them have proposed to specifically review phase diagrams' establishment and interpretation. We quickly fill this gap here.

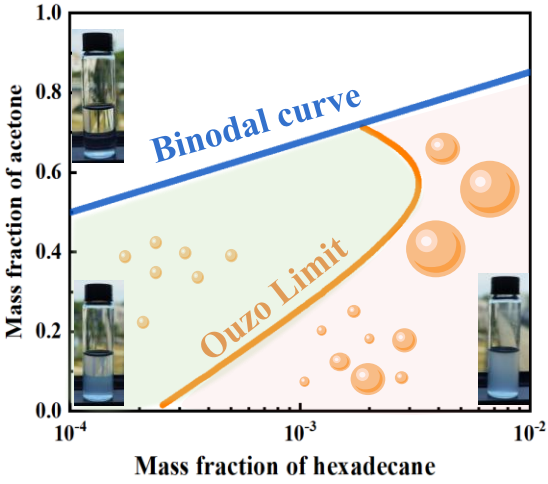

Figure 1. Typical phase diagram derived in Ouzo effect. Above the binodal line, the samples are transparent (even if microemulsions can be tracked for different solutes, not described here). In the Ouzo domain (in green), colloids of same distribution size are obtained in the full volume whereas, beyond the Ouzo limit (in orange), polydisperse samples with

large microdroplets are generated. Photos are hexadecane/acetone/water dispersions in the various domains.

Table 1: Brief survey of studies that reported Ouzo like phase diagrams. Here, only solutes and solvents that produced a full diagram are given. More is generally available in the papers.

Type	Solute	Solvent	Surfactant	Characterization technique	Other techniques	Reference
polymer	PCL	Acetone	none	Number of counts (DLS) Size measurement	TEM	13
	PLGA PLGA-co-vinyl sulfonate	Acetone	Pluronic F68	Visual inspection (immediate)	Particle size by DLS Surface charge by Zetametry Morphology by AFM	14
	PMMA	Acetone THF	Brij 56	Number of counts (DLS)	Size measurements TEM	10
	PLGA	THF DMSO	Pluronic F68	OD before and after filtration	Particle size by DLS Morphology by TEM	15
	PLGA	Acetone THF	Pluronic F68	OD before and after filtration	Particle size by DLS	16
	poly(4-vinylphenol-alt-alkylmaleimide	THF	none	OD vs concentration	Morphology by SLS, SANS and (cryo)TEM	17
Oil	BHT	THF	None Particles	Visual inspection (1h)	particle size by NTA DOSY NMR	18 19
	Anethol	Ethanol	none	Visual inspection	Droplet size by DLS Surface tension measurements	20
	DVB	Ethanol	None	Size of particles	none	5
	PETRA	Ethanol	none	Visual inspection (time not given)	Particle size by DLS Polymerization of the monomer	21
	Toluene	Ethanol	None SDS (post addition)	Visual inspection (1h)	Stability + average size by Turbiscan Aging by Diffusometry NMR	22
	Perfluorohexane	Propanol	none	Size measurement	particle size by NTA	23
	Hexadecane	Acetone	Brij 56	Number of counts before and after filtration	Size measurement	7
	Miglyol 812	Acetone	Brij 56	Number of counts before and after filtration	Size measurement	8
	Trilaurin	Acetone	none	Visual inspection	Microfluidic determination of PD	24
others	Condensed trialkoxysilane (MPTMS)	DMSO	none	Visual inspection (24h)	Particle size by DLS Morphology by TEM	25
	DSPE-PEG	THF	none	Particle size measurement	SEM, Fluorescence (with dye)	26, 27

Abbreviations: PCL: poly(caprolactone); PLGA: poly(lactid-co-glycolide acid); PMMA: poly(methylmethacrylate); BHT: butylated hydroxytoluene; DVB: divinylbenzene; PETRA: Pentaerythritol tetraacrylate; MPTMS: (3-mercaptopropyl)trimethoxysilane; SDS: sodium dodecyl sulfate; DLS: diffusion light scattering; NTA: nanoparticle tracking analysis; NMR: nuclear magnetic resonance; TEM: transmission electron microscopy; SANS: small angle neutron scattering; AFM: Atomic force microscopy; DSPE-PEG: 1,2-distearoyl-sn-glycero-3-phosphoethanolamine–polyethylene glycol.

We will not focus on the binodal line, that is easily determined by visual observation through a 'titration' method: basically, water is poured drop by drop in a solution of solute until the mixture becomes cloudy. This step is done at various solute concentrations to draw the binodal line (Fig. 1). On the other hand, the Ouzo limit is far more difficult to track, mostly because cloudy mixtures are generated both below and above the Ouzo limit (with larger objects generated beyond the limit, generally not seeable by the eye). In the case of polymers, the generated (solid) objects remain as they are once precipitated, whereas for oils and solid molecules, the system continues to evolve via Ostwald ripening and/or coalescence and crystallization into eye-observable threads, respectively. Table 1 cites the works that have specifically derived phase diagrams for a variety of solutes as described below (not including solid lipid nanoparticles[28]).

2.1 The 'easy' case of polymers

Most reports have shown phase diagrams of (co)polymers precipitated using different solvents. In one author's previous review, an update of particle generation by nanoprecipitation was made back to 2005.[2] Since then, various studies have shown polymer phase diagrams determined mostly by DLS or turbidimetry (see Table 1). It consists in reporting the number of counts or optical density, respectively, as a function of final polymer concentration: once the Ouzo limit is crossed, large aggregates separate from the mixture and these values decrease. Since particles are solid and do not evolve once formed, other characterization techniques were used to confirm the shift, mainly size measurements by DLS or various microscopies. It is worth mentioning the works of Beck-Broichsitter et al on PLGA and derivatives: the first visual phase diagram[14]

was later revised into a new diagram obtained by (more accurate) DLS results[16].

2.2 Other 'complex' solutes

Ouzo effect can be applied to any types of solutes, including in first hand oils. Many reports have recently been done on phase diagram establishment to reveal the Ouzo zone (Table 1). Most studies only relied on visual observation, with a high level of uncertainty on the limit determination. Even when DLS was used, for instance by recording the number of counts before and after filtration, data were scarcely distributed. The reasons for that are basically the strong propensity of droplets to coalescence and ripen with time, particularly in a mixture of solvent and water.

The addition of surfactant to stabilize the colloids would certainly be helpful here, but affects the measurements as well. Phase diagram of thiolated alkoxysilane and pegylated lipid has recently been proposed, with also a high level of uncertainty with respect to the reactivity and amphiphilicity of these solutes, respectively.

3. Experimental part

3.1 Materials

Unless otherwise stated, all reagents were purchased from Sigma Aldrich and used as received. Hexadecane, (reagent plus, 99%), hexadecanethiol (for synthesis, ≥88%), oleic acid (technical grade, 90%, traces of BHT), olive oil (technical grade, 90%), soybean oil (dietary source of long-chain triglycerides and other lipids, Laboratory reagent grade), miglyol 812 (IOI oleo Gmbh) and saturated medium chain triglycerides (Labrafac WL1349, Laboratory reagent grade, Gatefossé SAS) were selected as solutes of interest. Deionized water of 18.2 MΩ/cm was produced on a Double Column Véolia Water technologies device. Acetone, ethanol and isopropanol were all ≥99.9% purity. Pyrene (98%) was used as a tracer for fluorescence microscopy measurements, and Brij 56 as a surfactant in DLS analyses. Hydrochloric acid and sodium hydroxide (for analysis, Carlo Erba reagents) were used to modify the pH of the aqueous solution prior precipitation.

3.2 Methods

Fluorescence microscopy was performed on a Carl Zeiss AxioImager A1 DIC equipped with a fluorescent unit (Oberkochen, Germany). The objective lens was set to 10X magnification, and the filter position allowing 300 to 390 nm excitation selected. The measurement was performed on fixed slides with fresh solutions and 2 s exposure time for controlling the quality image.

DLS was performed on a Zetasizer nanoseries from Malvern instruments. The attenuator index and measurement position were automatically adjusted by the apparatus, whereas the detector position was set at 175° (back-scattering measurement). Different diameters were obtained, depending on the theory and assumptions made while fitting the diffusion signal. On one hand, the intensity diameter (d_I) is a fair estimation of the overall average diameter assuming a Lorenzian distribution. On the other hand, the volume distribution (d_V) assumes that the Mie theory applies (which is generally the case in such diluted dispersions). These two latter dimensions are compared to track the apparition of large droplets (vide infra).

3.3 Phase diagram determination

The binodal curve was generated as reported before[7,8] by titration with naked eye. Basically, water was added drop by drop into solutions displaying different concentrations of solutes until a precipitation occurs, denoting the limit between SFME domain (transparent solution, formation of thermodynamically stable aggregates at the nanometer scale) and the Ouzo domain (turbid solution, formation of a metastable emulsion). For very dilute solutions, the shift from clear to translucid states may not be observed, so concentrated enough solute solutions (typically above $5x10^{-4}$ wt.%) were privileged here[19].

The Ouzo limit was determined independently by fluorescence microscopy and light scattering. In the first technique, pyrene, fully soluble in the selected oils, was introduced in the organic solution prior to precipitation (typically 1.5 wt% compared to oil). The images were recorded right after solvent shifting, and were rated according to the spotting or not of large droplets in the sample. Practically, the formation of nanodroplets (in the Ouzo domain) is not detected by optical microscopy and results in the production of full dark images whereas beyond the Ouzo limit, large micrometric fluorescent droplets are easily pinpointed. An intermediary state was also noted, close to the Ouzo limit, where one can hardly see few micron-size droplets. In the case of large volumes of solvent (more than 40wt% acetone), pyrene diffuses out of the droplets and partition also in the dispersing medium, shutting down the fluorescence signal. Slow dilution of the samples with water brings back the pyrene in the droplets without affecting the droplet distribution, thus allowing to track the Ouzo limit at these solvent concentrations and generate a full phase diagram. All data points were reproduced three times.

Using light scattering, different parameters were tracked, namely the intensity mean diameter (d_I), the volume mean diameter (d_V) and the polydispersity index (PDI). As solvent shifting in the Ouzo domain typically gives birth to a single population of nanoparticles/nanodroplets with narrow size distribution, several criteria were then defined to separate samples prepared in the ouzo domain from those prepared in the heterogenous one: a given threshold for PDI (above 1.5), d_I size plots (where a second peak shows up), and crossing of d_I and d_V values (*vide infra*). Samples were freshly prepared in presence of surfactant at different concentrations (ratios of 0.2, 1 and 2 in Brij/oil in acetone) and diluted 10 times with water prior size measurements. Note that data became inconsistent for acetone concentrations above 0.5, so that the phase diagrams are generally truncated using this method.

4. Results

4.1. Phase diagram of hexadecane/acetone/water revisited

In a former publication[7], we have already determined the phase diagram of hexadecane/acetone/water ternary system. Titration and macroscopic observation derived the binodal curve. We also used DLS to monitor the scattered

intensity before and after filtration, as reported before for polymers, and plot the Ouzo limit. Whereas the binodal

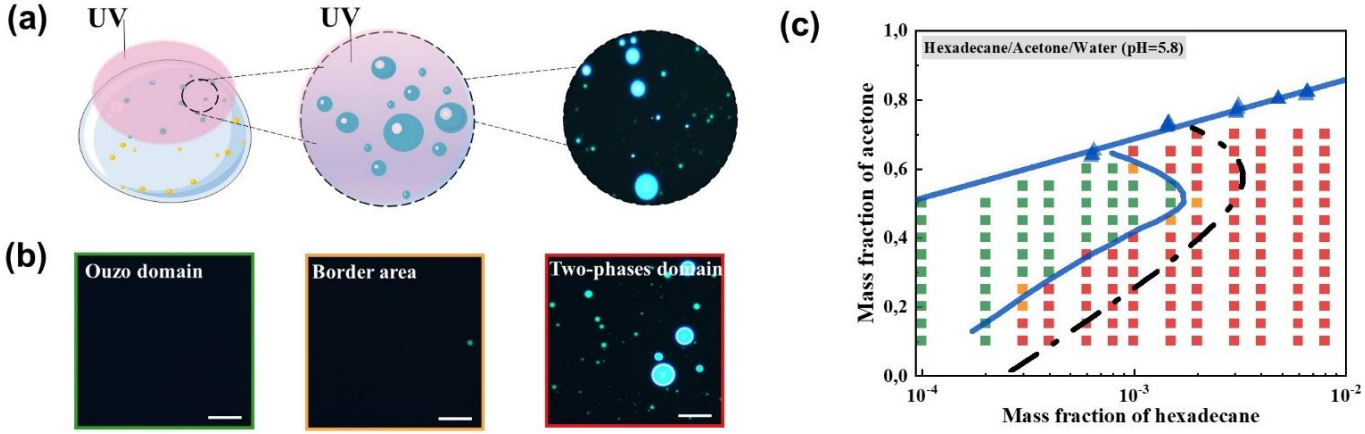

Figure 2. a) Principle of the Ouzo limit determination using fluorescence microscopy. The oil dispersions are loaded with pyrene that emits only in a strong hydrophobic environment; b) Corresponding photos. Below the binodal curve, the samples can come up at three different states: numerous big microdroplets in the heterogeneous state (beyond the Ouzo limit), a fully black sample in the Ouzo domain (before the Ouzo limit) or with very few small spots (at the edge of the Ouzo limit). Scale bar is 100 µm. See corresponding colored zones in Fig. 1; c) Phase diagram of HD/acetone/water as determined by FM. Black dashed-dotted curve corresponds to the previously derived Ouzo limit[7].

curve is a straight line that was invariably found at the same location, data were not perfectly aligned concerning the Ouzo limit and thus required further studying (see Fig. S1 for previous phase diagram and newly derived binodal curve superimposed).

4.1.1 Fluorescence microscopy

The principle of Ouzo limit determination by fluorescence microscopy is shown in Fig. 2a. Basically, a small content of pyrene was added in acetone phase prior to solvent shifting. This pyrene emits a strong fluorescence signal in hydrophobic surrounding such as inside oil droplets. Once the binodal curve is crossed, the solvent shifting produces either small nanodroplets or numerous, heterogenous droplets (see Fig 1). Accordingly, the microscopy thus shows no spot in the Ouzo domain (nanodroplets are too small to be seen) or big fluorescent spots of various sizes in the heterogenous domain (Fig. 2b). We have also defined an intermediate state, with very few micron-size droplets (Fig. 2b). These data are respectively reported in the phase diagram in green, red and orange, respectively.

Fig. 2c shows the phase diagram of HD/acetone/water as determined by this technique (all fluorescence microscopy photos are available in Fig. S2). The Ouzo limit follows the border between Ouzo domain (in green) and heterogeneous domain (in red). The curveted shape is typical of this representation in 2D graphs, as observed previously[10]. This phase diagram was also tracked in absence of pyrene (optical microscopy), and gives similar results, although it is then far more difficult to separate the droplets from eventual impurities or air bubbles (Fig. S3). We also checked that in presence of a surfactant, such technique was not successful, because most droplets, even in the heterogeneous domain, would be too small to be observed properly by optical microscopy.

In Fig. 2c, we report as well the Ouzo limit as it was determined previously. Clearly, the present FM technique is able to better locate the transition from the Ouzo domain to the heterogeneous one than before (compare with Fig. S1). It is also a simple and rapid procedure, that allows one to draw a full phase diagram in typically one day or so. It is also a surfactant-free method, contrary to DLS procedure. We elaborate on this difference below.

4.1.2 Dynamic light scattering

A second technology largely used by the soft matter community measures droplet sizes by light scattering. In these experiments, we introduced a surfactant, as done before[7], to ensure that the droplets would be stable enough on the long run to perform size measurements (Brij 56, initial ratio of 2 to 1 compared to HD, introduced in the organic phase). Contrary to what was done before, we did not filter the dispersions to estimate the Ouzo limit, but proposed a triplicate estimation based on raw data (Fig. 3, exemplified with data gathered at 10 wt.% acetone): 1. d_I and d_V are not similarly affected by the presence of large aggregates: if d_V gets larger than d_I then the ouzo limit is crossed (Fig. 3a); 2. Looking at the intensity size distribution, we separate the Ouzo domain where only one peak is observed from the heterogeneous domain where a second peak shows up (Fig. 3b); 3. The polydispersity of the intensity signal broadens while crossing the Ouzo limit to get larger than 1.5, a threshold value that we have chosen as representative of the shift between Ouzo domain and heterogeneous phase (Fig. 3c). Samples in and outside Ouzo domain are shown by the green and red bars on the top, respectively.

All the data obtained at different acetone/water ratio are available in Fig. S4. The corresponding phase diagram is reported in Fig. 3d, again showing up as green and red data. Thanks to the data crossing from the three criteria of Ouzo limit determination, there is no doubt on the Ouzo limit location, so orange plots are no more needed here. The Ouzo limit is drawn in blue and is slightly shifted from previously derived one (dash-dot black curve).

In the Ouzo domain, the average size of the droplets can be plotted as a function of HD concentration and different acetone:water ratio (Fig. 3e). All measurements follow a

line as a function of solute concentration, with the exception of those gathered at 50wt.% acetone for non-obvious reasons

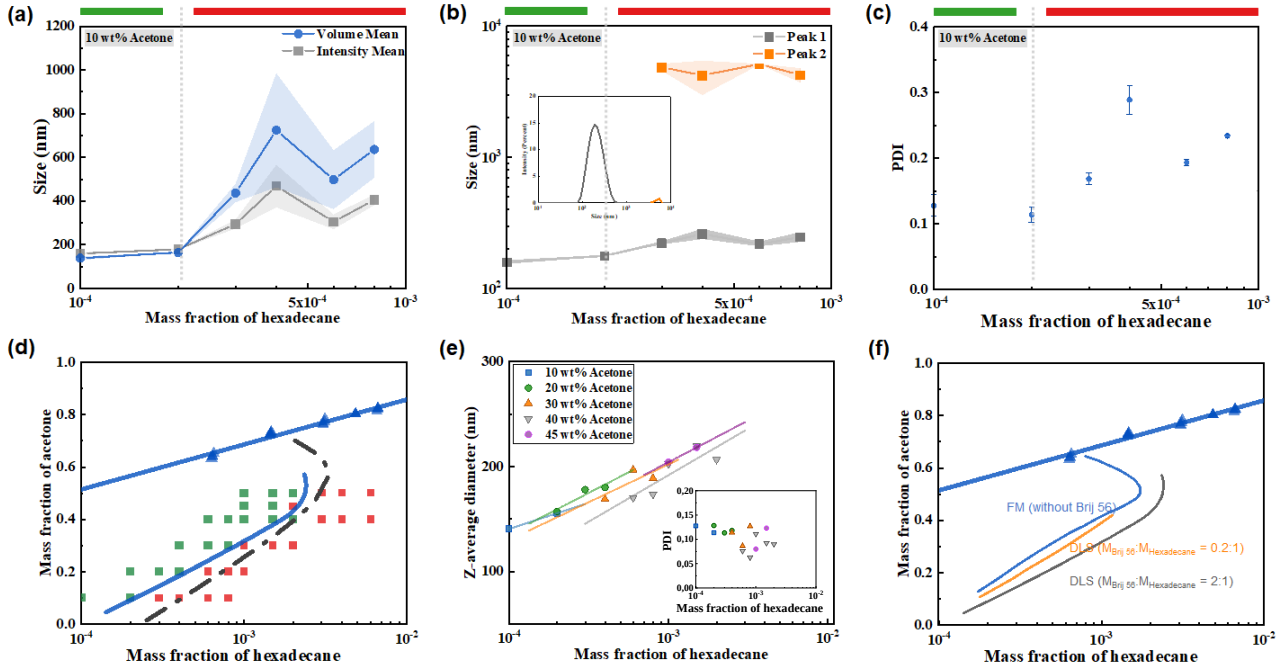

Figure 3. a-c) Overview of the new DLS-based procedure to measure the Ouzo limit in the hexadecane/acetone/water system, exemplified here with the testing at 10 wt.% acetone and increasing HD concentration; green zone indicates Ouzo domain and red one the heterogeneous domain: a) Size in volume and intensity means versus HD content; the crossover between the two indicates the generation of large droplets, formed in the heterogeneous phase; b) apparition of a second peak when crossing the Ouzo limit (see in inset the corresponding intensity size distribution generated by DLS); c) evolution of polydispersity index with HD content, and the crossing of the 1.5 arbitrarily-chosen threshold; d) Phase diagram of HD/acetone/water as determined by the new DLS-based procedure, following the same presentation than in Fig. 2c. Black dashed-dotted curve corresponds to previously derived Ouzo limit with previously reported -DLS-based procedure[7]; e) size evolution versus HD content at different final acetone content; all data mostly line up except experiments done at 50 wt.% acetone (Fig. S5). Inset: PDI of the corresponding droplets; f) influence of the content of Brij56 on the determination of the Ouzo limit, compared to the FM-generated curve (see full data in Fig. S6).

(see data in Fig. S5). The increase of size with HD concentration is expected from the nucleation and aggregation theory. The range of droplet diameters is quite narrow and mostly imposed by the presence of surfactant originally in the organic phase.

4.1.3 Comparison of the two techniques

From Fig.2c and Fig. 3d, it is quite clear that the Ouzo limit is not located at the same place whether FM, previously reported-DLS or new-DLS procedures are used. First, the new procedure proposed by DLS is more robust than the previously derived one because of the self-consistency the three measured parameters show. We also do not filter the samples, thus avoiding uncontrolled coalescence of the droplets.

To understand the discrepancies between FM and new DLS technique, we have performed new experiments where the content of Brij56 was varied (Fig. 3f shows only the final result, see data in Fig. S6). Experiments done at 0.2:1 ratio of Brij56:HD practically overlap with FM results in terms of Ouzo limit. Note that the sizes of the droplets again show an increase with HD content, and are lower in average at 1:1 and 2:1 ratio than at 0.2:1 (Fig. S7).

Note that the surfactant must be inserted in the organic phase to optimize the generation of nanodroplets and their stability; adding Brij56 in water basically does not allow forming measurable droplet distribution (not shown). This is ascribed to the fact that the kinetics of droplet formation is so fast that the surfactant must be on-site to adsorb to the generated interfaces rapidly and stop the droplets aggregation process[29].

4.2 Application to other phase diagrams

To illustrate the simplicity of these new procedures, we next made use of the easy to handle fluorescence microscopy procedure to derive a series of phase diagrams where the nature of solvents, oils (including mixtures) and external conditions (mostly pH) were varied. Full diagrams will all data are given in Fig. S8, we report here exclusively the binodal and Ouzo boundaries, whereas droplet sizes were obviously not measured.

4.2.1 Variations around hexadecane nanoprecipitation

It was shown before for the nanoprecipitation of polymers that the type of solvent used could have a strong impact on the location of the Ouzo limit (Julien Nicolas, others?). Fig. 4a shows the phase diagrams of hexadecane solubilized in ethanol and isopropanol, to be compared with previous data with acetone (Fig. 4a).The binodal curves overlap for ethanol and acetone, but is much lower in concentration for isopropanol. This is a priori explained by the better affinity of oil for isopropanol. The Ouzo limits basically fall on the same concentration range. We also looked at the

effect of pH on phase diagram of hexadecane/acetone/water. Neither the binodal nor the Ouzo limits are basically shifted here (Fig. S9). The largest Ouzo domain is at neutral pH.

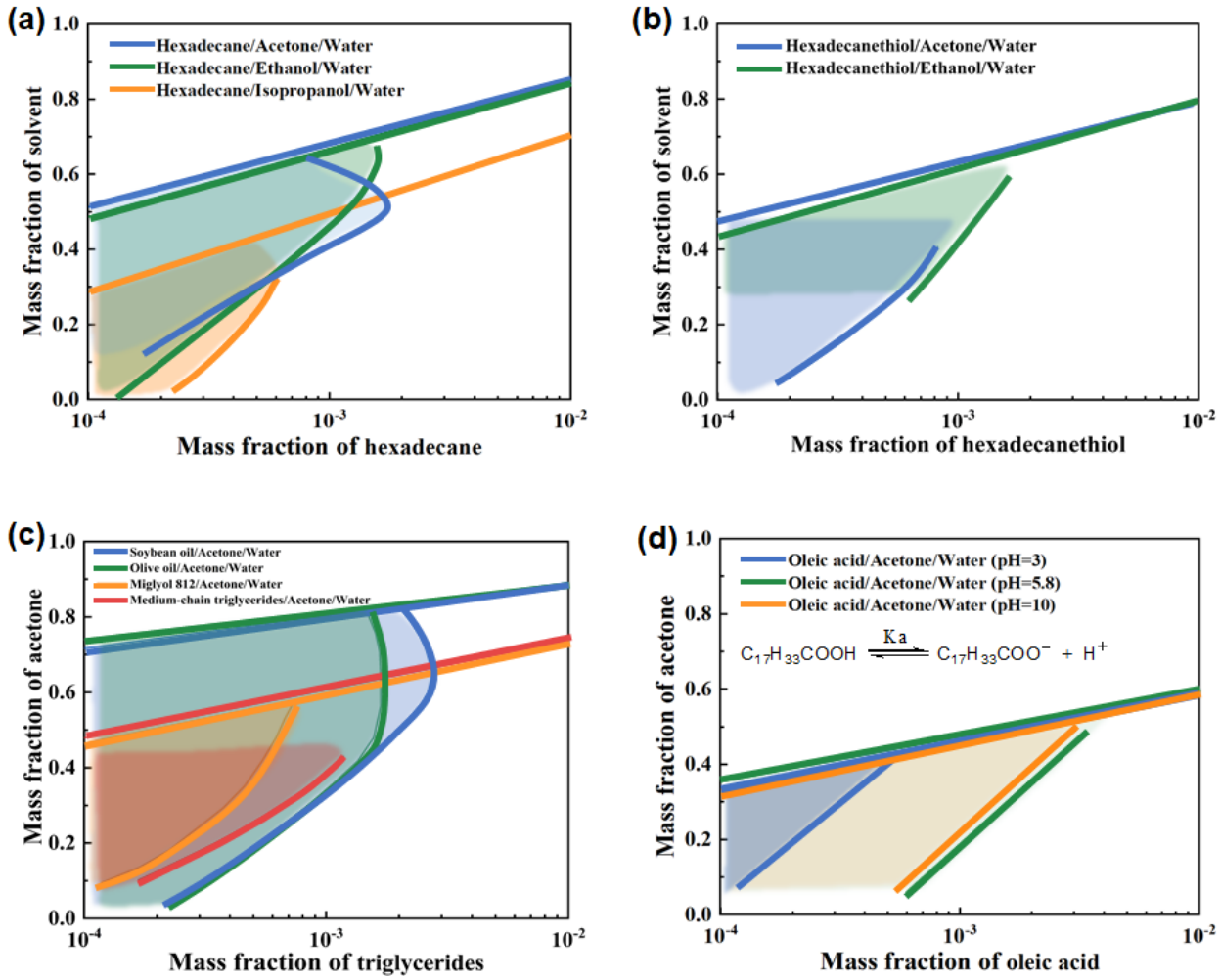

Figure 4. Simplified phase diagrams for different oils studied here by FM (diagrams with full data are available in Fig. S8). a) influence of the nature of solvent on the PD of hexadecane; b) hexadecanethiol PDs in two solvents; c) triglycerides of different natures versus acetone; d) oleic acid PDs in acetone as a function of pH; d) oleic acid PDs in acetone as a function of pH. Inset shows the classical equilibrium of this fatty acid (pKa is about 4.5).

4.2.2 Other conventional oils

Hexadecanethiol is an interesting functional oil that could be used as precursor for prodrugs nanoprecipitation. We have evaluated its phase diagram starting from acetone and ethanol solutions (Fig. 4b). The Ouzo domain is very similar to the HD one, thus not showing any effect of the functionality on the physical chemistry of nanoprecipitation. This is quite different from what has been observed previously for polymers, where the ionic nature of the chain-ends greatly affects the PDs[13,30].

Gauffre et al[19] have shown before that coprecipitation of oils could be performed with confidence, once the respective phase diagrams were shown. Here, we have mixed HDT and oleic acid in a 50:50 ratio and measured the co-phase diagram (Fig. S8). As expected, the boundaries are seen in between those of the two independent solutes' ones. Most likely, the oleic acid must partition preferentially at the interface (*vide infra*).

Triglycerides are natural oils that are extensively used in cosmetics, drug delivery or food excipients. We compare in Fig. 4c the phase diagrams of Miglyol (already derived in a previous paper from us[8]), olive oil, soybean oil and medium chain triglycerides. Miglyol boundaries are very close from those derived before by DLS (Fig. S10), again with a slight shift according to the precision of the measurements. Medium chain triglycerides are C8-C10 saturated chains, very similar to Miglyol, and so is the phase diagram. Olive oil and soybean oil are larger molar mass triglycerides with higher hydrophobicity. Their corresponding phase diagrams are larger, with a binodal curve location quite high on the y axis, and a slightly shifted Ouzo limit towards larger oil concentrations.

4.2.3 The specific case of oleic acid

Oleic acid is another fatty acid largely used as a model oil in aqueous dispersions. It is also useful as ligands to stabilize nanoparticles, thanks to its pH-sensitive amphiphilicity. Fig. 4d shows the phase diagrams of oleic acid in acetone performed at different pHs. Binodal curves are basically independent of the pH. On the contrary, the Ouzo limit is highly impacted by the pH. At pHs above the

pKa of the acid, the presence of ionic groups on the droplets surface help to nanoprecipitation, with a maximum mass fraction of oleic acid of about 10^{-2}.

Since droplets thus formed are stabilized by carboxylate groups, it is possible to observe their size in DLS without the need for a surfactant. Fig. S11 shows that for final acetone content of 10 and 30 wt.%, sizes evolve on the same line between 125 and 230 nm. We did not manage to report a phase diagram as the 3 consistency tests of the DLS technique were not respected here (not shown).

5. Discussion

What makes the Ouzo effect popular nowadays in the physical chemistry community is the easiness with which one can prepare dispersions of many different solutes, especially since rationalization of the phase diagrams has been proposed by Vitale and Katz. The difficulty not alleviated yet is the high dilution required for full-volume nanoprecipitation, with a maximum final concentration of solutes in the dispersion of typically 1 wt.%. Understanding the process of nucleation, aggregation and stopping events is key to simulate the location of the Ouzo limit and hopefully shift it towards larger solute concentration. This requires thorough experiments that have been described here, using two complementary techniques.

In all derived graphs, the binodal curve is independent of the external conditions of the process, as expected from a thermodynamically-controlled boundary. It depends mostly on the nature of the solvent, both in terms of initial solubility of the solute and rate of diffusion towards water during nanoprecipitation. Quite surprisingly, the binodal curve of oleic acid in acetone is low, meaning that large content of water is required to initiate the precipitation.

The curvy shape of the Ouzo limit generally observed comes from the opted binary diagram and log-scale of the x axis. The Ouzo limit is kinetically controlled, since it shifts with the conditions of precipitation. Its location depends on pH or the addition of surfactant, both susceptible to interact with the aggregation process. Since FM is carried out in absence of surfactant, and DLS is done with Brij56, limits are not overlapping for HD. Nevertheless, limiting the surfactant content almost brings back these limits together.

Fessi and coworkers[13] have proposed in 1995 a simple trick to linearize the Ouzo limit in the PCL/acetone/water system, and that we have also later applied to PMMA polymer precipitated from THF and acetone. It consists in plotting the initial concentration of solutes as a function of the solvent/water ratio at which the Ouzo limit is crossed (with a limitation of a ratio of 1.2 as preconized by Fessi and coworkers). We have done the same for the triglyceride oils and hexadecane, as well as anethole from a previously published phase diagram[20]. The linear curves are plotted Figure 5 (full data are given in Figure S12).

One evident feature of this graph is that the linear curves do not show the same slopes according to the type of solutes. Polymers give negative slopes, whereas oils give positive or flat slopes (the limited data for soybean and olive oils do not allow discriminating clearly on this point). This observation seems to indicate that the STOP event in aggregation[29] is not the same for polymer particles or oil droplets. We have shown before that polymer nanoprecipitation is highly dependent on the bicarbonate adsorption on the interface,[31] those ions coming from the CO_2 content

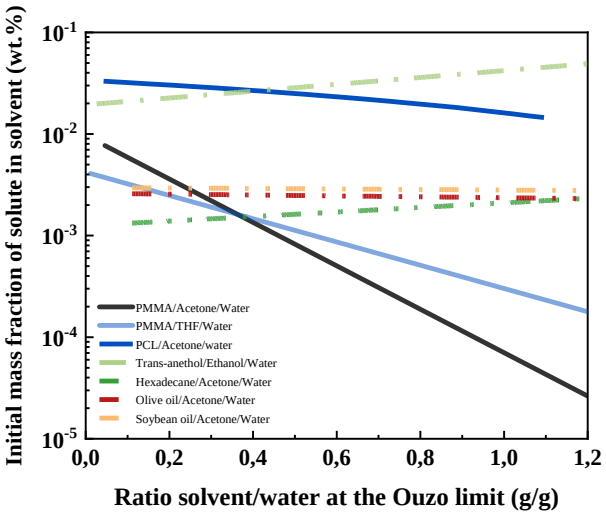

Figure 5. Linearization of the Ouzo limits for different polymers (plain lines) and oils (dash-dot-dot lines) according to Fessi's procedure. For references on the data not collected here, please see the main text.

in the solvent and directly present in the water phase. The larger the initial content of solutes in the solvent, the larger water content to add to reach the Ouzo limit. This is not the case for oils that are less sensitive to bicarbonate adsorption; here instead, the Ouzo limit occurs for a constant initial concentration of solutes.

Another fact from this graph is the different locations of PCL[13] compared to PMMA[10] lines, and anethol[20] compared to HD and triglyceride oils. This actually also corresponds to data collected by us and others, respectively. We do not know if such discrepancies come from the way of measuring the Ouzo limit, or if this trend is real. Since PCL have chain-ends that can be ionized, the higher content of precipitated solute is readily understandable. For the anethol superior curve, this is not straightforward as the authors have worked on very pure solute (only traces of non-amphiphilic molecules) and in absence of surfactant. Final concentrations of dispersions are about 10 times larger than for our best shot, oleic acid that is amphiphilic. It would be interesting to redo this phase diagram with our current PD determination technologies.

6. Conclusion and prospects

Fluorescence microscopy and dynamic light scattering are two complementary methods to track the Ouzo limit while nanoprecipitating oils. Both methods use an extra molecule, namely a fluorophore and a surfactant, respectively. Still, the accuracy with which the data are obtained is much better than done before, albeit for oils (it is easier for polymers).

The physics of the STOP event for aggregation is still to be unraveled. This is the condition to find the right formulations that will shift the Ouzo limit towards larger final

dispersion concentrations. Whereas this is straightforward with polymers by introducing ionic groups in the chains, this is not possible for oils unless adding a complementary component such as a surfactant. In a following communication we will show that precisely chosen ones can indeed enlarge the Ouzo domain better than done so far.

ASSOCIATED CONTENT

Supporting Information. Phases diagrams with full data; FM images; DLS results; Particle size variations; Full data of linearization plots. This material is available free of charge via the Internet at http://pubs.acs.org.

AUTHOR INFORMATION

Corresponding Author

* Dr François Ganachaud. Tel: +33 6 83 02 18 02. Mail: francois.ganachaud@insa-lyon.fr; Dr Julien Bernard. Mail: Julien.bernard@insa-lyon.fr

Author Contributions

All authors have given approval to the final version of the manuscript.

ACKNOWLEDGMENT

Y.C. thanks CSC for her Ph. D. grant.

ABBREVIATIONS

DLS, dynamic light scattering; FM: fluorescence microscopy; PD: phase diagram.

REFERENCES

(1) Horn, D. & Rieger, J. Organic Nanoparticles in the Aqueous Phase-Theory, Experiment, and Use. Angew. Chem. 40 23, 4330–4361 (2001).

(2) Ganachaud, F. & Katz, J. L. Nanoparticles and Nanocapsules Created Using the Ouzo Effect: Spontaneous Emulsification as an Alternative to Ultrasonic and High-Shear Devices. ChemPhysChem 6, 209–216 (2005).

(3) Lepeltier E., Bourgaux C. & Couvreur P. Nanoprecipitation and the “Ouzo effect”: Application to drug delivery devices. Adv. Drug Deliv. Rev. 71, 86–97 (2014).

(4) Botet, R. The" ouzo effect", recent developments and application to therapeutic drug carrying. in Journal of Physics: Conference Series 352, 012047 (2012).

(5) Vitale, S. A. & Katz, J. L. Liquid Droplet Dispersions Formed by Homogeneous Liquid–Liquid Nucleation: “The Ouzo Effect”. Langmuir 19, 4105–4110 (2003).

(6) Yan X, Bernard J, Ganachaud F. Nanoprecipitation as a simple and straightforward process to create complex polymeric colloidal morphologies. Adv Colloid Interface Sci. 294, 102474 (2021).

(7) Yan, X. et al. Simple but Precise Engineering of Functional Nanocapsules through Nanoprecipitation. Angew. Chem. Int. Ed. 53, 6910–6913 (2014).

(8) Yan, X. et al. Brilliant glyconanocapsules for trapping of bacteria. Chem. Commun. 51, 13193–13196 (2015).

(9) Yan, X. et al., Modular construction of single-component polymer nanocapsules through a one-step surfactant-free microemulsion templated synthesis, Chem. Commun. 53, 1401–1404. (2017).

(10) Aubry, J., Ganachaud, F., Cohen Addad, J.-P. & Cabane, B. Nanoprecipitation of Polymethylmethacrylate by Solvent Shifting:1. Boundaries. Langmuir 25, 1970–1979 (2009).

(11) Ding S, Anton N, Vandamme TF, Serra CA. Microfluidic nanoprecipitation systems for preparing pure drug or polymeric drug loaded nanoparticles: an overview. Expert Opin Drug Deliv. 2016 Oct;13(10):1447-60.

(12) Walid S. Saad, Robert K. Prud’homme, Principles of nanoparticle formation by flash nanoprecipitation, Nano Today, 11, 212-227 (2016).

(13) Stainmesse, S., Orecchioni, A.-M., Nakache, E., Puisieux, F. & Fessi, H. Formation and stabilization of a biodegradable polymeric colloidal suspension of nanoparticles. Colloid Polym. Sci. 273, 505–511 (1995).

(14) Beck-Broichsitter, M., Rytting, E., Lebhardt, T., Wang, X. & Kissel, T. Preparation of nanoparticles by solvent displacement for drug delivery: a shift in the ‘ouzo region’ upon drug loading. Eur. J. Pharm. Sci. Off. J. Eur. Fed. Pharm. Sci. 41 2, 244–53 (2010).

(15) Beck-Broichsitter M, Nicolas J, Couvreur P. Solvent selection causes remarkable shifts of the "Ouzo region" for poly(lactide-co-glycolide) nanoparticles prepared by nanoprecipitation. Nanoscale 7, 9215-21 (2015).

(16) Beck-Broichsitter, M. Stability-limit Ouzo region boundaries for poly(lactide-co-glycolide) nanoparticles prepared by nanoprecipitation. *Int. J. Pharm*. **511**, 262–266 (2016).

(17) Trevisan, H. et al. Ouzo phase occurrence with alternating lipo/hydrophilic copolymers in water. Soft Matter 17, 7384–7395 (2021).

(18) Goubault, C. et al. Effect of nanoparticles on spontaneous Ouzo emulsification. J. Colloid Interface Sci. 603, 572–581 (2021).

(19) Iglicki D, Goubault C, Nour Mahamoud M, Chevance S, Gauffre F. Shedding light on the formation and stability of mesostructures in ternary "Ouzo" mixtures. J Colloid Interface Sci. 633, 72–81 (2023).

(20) Sitnikova, N. L., Sprik, R., Wegdam, G. & Eiser, E. Spontaneously Formed trans -Anethol/Water/Alcohol Emulsions: Mechanism of Formation and Stability. Langmuir 21, 7083–7089 (2005).

(21) Kempe H, Kempe M. Ouzo polymerization: A bottom-up green synthesis of polymer nanoparticles by free-radical polymerization of monomers spontaneously nucleated by the Ouzo effect; Application to molecular imprinting. J Colloid Interface Sci. 616, 560–570 (2022).

(22) Reza Tehrani-Bagha, A.; Viladot, A.; Holmberg, K.; Nordstierna, L.; An Ouzo emulsion of toluene in water characterized by NMR diffusometry and static multiple light scattering, *Colloids Surf. A: Physicochem. Engin. Asp.*, 494, 81-86 (2016).

(23) Ji, Y. et al, Controllable formation of bulk perfluorohexane nanodroplets by solvent exchange, *Soft Matter*, ,18, 425-433 (2022).

(24) Rosenfeld, J.; Ganachaud, F.; Lee, D. Nanocomposite colloids prepared by the Ouzo effect, *J Colloid Interface Sci.* **653**, 1753–1762 (2024)

(25) Shih-Jiuan Chiu, Su-Yuan Wang, Hung-Chang Chou, Ying-Ling Liu, and Teh-Min Hu, Versatile Synthesis of Thiol- and Amine-Bifunctionalized Silica Nanoparticles Based on the Ouzo Effect, Langmuir 30, 7676-7686 (2014).

(26) Middha E. et al, Direct visualization of the ouzo zone through aggregation-induced dye emission for the synthesis of highly monodispersed polymeric nanoparticles, *Mater. Chem. Front*., 3, 1375—1384 (2019).

(27) Middha, E., Chen, C., Manghnani, P. N., Wang, S., Zhen, S., Zhao, Z., Liu, B., Synthesis of Uniform Polymer Encapsulated Organic Nanocrystals through Ouzo Nanocrystallization. Small Methods 2022, 6, 2100808.

(28) Naseri N, Valizadeh H, Zakeri-Milani P. Solid Lipid Nanoparticles and Nanostructured Lipid Carriers: Structure, Preparation and Application. Adv Pharm Bull. 2015 Sep;5(3):305-13.

(29) Lannibois, H., Hasmy, A., Botet, R., Chariol, O. A. & Cabane, B. Surfactant Limited Aggregation of Hydrophobic Molecules in Water. J. Phys. II 7, 319–342 (1997).

(30) Roger, K.; Eissa, M.; Elaissari, A.; Cabane, B. Surface Charge of Polymer Particles in Water: The Role of Ionic End-Groups. Langmuir, 29, 11244-11250 (2013).

(31) Yan, X. et al Central Role of Bicarbonate Anions in Charging Water/Hydrophobic Interfaces. J. Phys. Chem. Lett. 9, 96-103 (2018).